

Research Article

DFT Investigation of Charge Transfer Complexes Formed between Naphthols with 1,3-Dinitrobenzene: Conformational, Structural, Electronic, Thermodynamic, and Spectroscopic **Insights**

Vahideh Hadigheh Rezvan^a, Hanieh Abdoli^b

^aDepartment of Chemistry, Ard. C., Islamic Azad University, Ardabil, Iran ^bYoung Researchers and Elite Club, Ard. C., Islamic Azad University, Ardabil, Iran

ABSTRACT

A charge transfer complex (CTC) is created through the interaction between a donor molecule and an acceptor molecule. This research explores density functional theory (DFT) investigations, focusing on the molecular structures, electronic properties, and spectroscopic analyses of CTCs formed by the interaction of 1-naphthol and 2-naphthol with 1,3dinitrobenzene. These complexes have not been synthesized; this study will aid in future experimental work. The study employs the B3LYP/6-311G(d,p) method to explore aspects like conformational analysis of naphthols, energy gaps between rotamers, molecular structures, electronic distributions, electric moments, thermodynamic parameters, frontier molecular orbitals (FMOs), molecular electrostatic maps, optical characteristics, UV-Vis, and IR spectroscopy analysis of CTCs in the gas phase. The conformational analysis of naphthols identified two rotamers, syn and anti, for both 1-naphthol and 2-naphthol. The energy gaps between these rotamers are small (-1.58 and 0.67 kcal/mol), allowing rapid interconversion at room temperature. Gas-phase optimized structures show only minor changes in bond angles, with very small variations. For both complexes, the naphthol bonding framework remains largely unchanged, though slight adjustments near the OH group occur (an OH-NO2 hydrogen-bond interaction is suggested by an ~0.003 Å elongation in certain distances). The acceptor fragment shows more pronounced changes, with a 0.007 Å increase in rNO and a ≈0.005 Å decrease in rCN, consistent with hydrogen-bond formation. Dihedral angles in the OH and NO2 regions (3-28 degrees) are particularly notable. UV-Vis analysis reveals new charge-transfer bands at 638 nm and 603 nm in the CT complexes, indicating electronic transitions. IR analysis shows 99 vibrational frequencies for the complexes, with band shifts linked to CT interactions. Thermodynamically, the interaction energy, enthalpy, entropy, and Gibbs free energy suggest limited stability and a non-spontaneous, exothermic formation. The interaction energies (-0.293 and -1.359 kcal/mol) imply only weak donor-acceptor coupling, consistent with CT complexes formed by weak intermolecular forces.

ARTICLE INFO

Received: 9 September 2025 Accepted: 6 November 2025 Available:13 November 2025

☑: V. Hadigheh-Rezvan Va.Hadigheh1344@iau.ac.ir



doi 10.82437/jcrs.2025.1217418

Keywords: Charge-transfer complex (CTC); NBO, 1,3dinitrobenzene; Naphthol; NLO; DFT; Rotamer; Electron-donor; Electron-acceptor.

Introduction

The chemical literature has documented many investigations into charge-transfer complexes (CTCs). CT interaction occurs when the charge moves from the donor to the acceptor, a concept proposed by Mulliken and further examined by Foster [1]. It is challenging to optimize and synthesize the CTC with intermolecular hydrogen bonds and exchange charges between donor and acceptor [2]. The color development in this intricate structure changes based on the acceptor's LUMO and the donor's HOMO interaction, which absorbs radiation in the visible range [3]. According to Pauling, this is an outstanding illustration of hydrogen bonding [4]. Atkins provided evidence for the existence of the dipole-dipole force in the complex. CTC is widely utilized in various aspects of human life because it possesses multiple biological and physicochemical resources. The CTCs have been used in numerous non-linear optical (NLO) materials [5-7], photocatalysts [8], electrical conductors [9], semiconductors [10], chemo-sensors [11], medicine [12], and various biological applications [13]. They are also employed for enzyme catalysis, insecticide purposes, antibacterial ion transfer, DNA-binding, and antifungal activities across lipophilic membranes [14].

A study on computational methods investigated the formation of CTCs between 1-hydroxypyrene and aromatic amino acids (phenylalanine, tyrosine, and tryptophan) when subjected to light in both gas and water [15]. DFT was employed to optimize the geometries of these CTCs using the xB97XD/6-311++G (d, p) theoretical framework. TD-DFT was used to analyze the electronic transitions of molecules based on the ground-state geometries obtained from xB97XD/6-311++G (d, p) at B3LYP/6-311++G (d, p) and CAM-B3LYP/6-311++G (d, p) levels. The creation of CTCs involving 2-amino-4-methoxy-6-methylpyrimidine, 2-amino-4-chloro-6-methylpyrimidine, and 2-amino-4,6-

dimethylpyrimidine as donors, along with chloranilic acid as the acceptor, was examined through spectrophotometric and conductometric techniques [16]. The absorption spectra in the solution were examined for CTCs created by 2,3-dichloro-5,6-dicyano-p-benzoquinone, p-acetotoluidide, acetanilide, biphenyl, and naphthalene. A spectral analysis of these substances was performed, and the ionization potential was compared with the donor [17]. The interaction between 8-hydroxyquinoline and 1,4-benzoquinone has been investigated in both solution and solid states. IR spectroscopy indicates that a CT interaction between these donors and acceptors occurs via $\pi \rightarrow \pi^*/n \rightarrow \pi^*$ transitions, leading to the formation of radical ion pairs [18]. A straightforward and highly sensitive method for quantitatively detecting 4-aminobenzoic acid is described. The technique relies on the interaction of 4-aminobenzoic acid acting as an electron donor with 2,3-dichloro-5,6-dicyano-1,4-benzoquinone serving as an acceptor, resulting in a brightly colored complex at a 1:1 ratio [19].

Charge-transfer assemblies, formed through donor–acceptor interactions, have found widespread use across electronics, optics, sensing, and catalysis. Unlike many assemblies that rely on covalent bonding, CTCs are driven by diverse intermolecular forces—primarily electrostatic interactions and charge transfer—that promote orderly packing. Their nanowire morphologies have important implications for next-generation organic electronic and optoelectronic devices, where they can serve as nanoscale channel materials. The two-component nature of CTCs yields unique, tunable physicochemical properties that are hard to achieve in single-component systems. Advantages of CTCs include scalable processing, low weight, reduced cost, and better compatibility with flexible platforms compared to inorganic alternatives. The emergence of these new states, distinct yet linked to the parent molecules, enables the tuning of electronic properties to span a spectrum of charge-transport behaviors, ranging from semiconducting to conducting and even superconducting regimes [20-23].

Ciprofloxacin (CIP) is widely used to treat a range of bacterial infections. Recent work has suggested potential anticancer properties, prompting broader exploration of its pharmacological effects. In solution, CIP forms a strong 1:1 complex with the acceptor, accompanied by a characteristic color change that provides initial evidence of charge-transfer complex (CTC) formation. The in vitro toxicity of this complex was evaluated with the MTT assay on a human carcinoma cell line, and the LD50 values were determined. Hematological and biochemical analyses were performed on blood samples, liver tissues were collected for further study [24].

Naphthols (1-naphthol and 2-naphthol) are essential intermediates, extensively employed in the manufacture and synthesis of dyes, synthetic rubbers, pesticides, and pharmaceutical industries [25-27]. Nevertheless, naphthols are widely recognized to have harmful effects on the environment and human health [28, 29]. 1-Naphthol (1-NP) or α-naphthol is a solid that emits white fluorescence. 1-NP is used as a starting material for many insecticides, such as carbaryl, and drugs like nadolol. 2-Naphthol (2-NP) or β-naphthol is a colorless crystalline solid that fluoresces. 2-NP is more harmful than 1-NP, causing severe systemic poisoning and potential damage to the liver and kidneys in humans through effects on blood circulation. Hence, it is crucial to create sensitive techniques for detecting both naphthols. Various methods, including gas chromatography-mass spectrometry [30], high-performance liquid chromatography [31], fluorescence spectrometry, electrochemical techniques [32], and capillary electrophoresis [33] have been developed to detect naphthols. Due to low pollutant levels and complex sample matrices, direct analysis is challenging. Therefore, greater emphasis is placed on improving sample pretreatment technologies. Recently, different methods of pretreatment have been created, with liquid-phase extraction and solid-phase extraction being the most frequently used methods for pretreating aqueous samples [34–36]. Solid-phase extraction is receiving a great deal of interest due to its ease, high recovery rates,

strong enrichment capabilities, and reduced use of harmful solvents [37]. Some methods are based on CT complexation reactions of naphthols with acceptors such as chloranil and DDQ. Several research groups have reported that 1,3-dinitrobenzene acts as an acceptor in the formation of CTC with phenols and other donor molecules.

1,3-Dinitrobenzene (*m*-**DNB**) or *m*-dinitrobenzene is utilized in different ways, such as being an intermediate in creating dyes and pigments, in pharmaceutical synthesis, and as a reagent in analytical chemistry. The toxicity and environmental persistence of *m*-**DNB** are major concerns due to its potential harm when inhaled or absorbed through the skin. It is recognized for its durability and ability to remain in the surroundings, resulting in possible soil and water systems buildup. Various methods can detect and measure *m*-**DNB**, including GC, HPLC, and titration. Utilizing a CTC formation approach to study *m*-**DNB** offers valuable insights into its characteristics and relationships. The development of CTC will generally lead to distinct absorption bands that can be utilized to validate the interaction. The use of CTCs to analyze *m*-**DNB** can help in measuring it in different samples and also in gaining insights into how it reacts with other compounds. These analyses are essential for monitoring and regulations due to their impacts on the environment and health.

In this article, we have reported the CTCs of naphthols as donors with 1,3-dinitrobenzene as π -acceptor. These CTCs are formed by the interaction between **1-NP** or **2-NP** and **m-DNB** (Scheme 1). This reaction can be used to detect naphthols and **m-DNB**. Theoretical calculations of these complexes with the DFT/B3LYP/6-311G(d,p) method have been done. Structural parameters, formation mechanism, IR and UV–Visible spectra, frontier molecular orbitals, optical properties, NBO analysis, and several other properties for these complexes were discussed. The study highlights the importance of CT in determining optical characteristics and suggests potential applications in nonlinear optics and materials science. While some studies discuss the formation of CTCs involving naphthols, detailed mechanistic

investigations are often lacking. Understanding the step-by-step processes of CT is crucial for a complete understanding of these complexes. There is a gap in exploring practical applications of naphthol-dinitrobenzene CTCs in science, such as organic photovoltaics, sensors, or NLO materials. By elucidating these molecular interactions and properties, this work contributes valuable insights into the fundamental understanding of CTCs and their applications in various fields.

The choice of the B3LYP functional with the 6-311G(d,p) basis set for DFT calculations in CTCs is popular for several key reasons: **i.** B3LYP is a hybrid functional that combines the Hartree-Fock exchange energy with a portion of the local density approximation (LDA) and generalized gradient approximation (GGA) correlation. This makes it relatively accurate while still being computationally efficient, which is advantageous for studying CT phenomena. **ii.** B3LYP has yielded reliable results for various electronic properties and is particularly adept at describing systems with significant CT characteristics. **iii.** The 6-311G(d,p) basis set allows for a more accurate description of electron correlation effects compared to smaller basis sets. **iv.** The combination of B3LYP with the 6-311G(d,p) basis set has been widely used and tested across many different systems, providing a reliable benchmark for comparison. This makes it a trusted choice for many researchers in the field.

DFT Calculations

DFT, a quantum mechanical technique, offers a more reliable structure than classical methods. All calculations were performed using Gaussian09 software [38] running on a PC with an Intel Core i5 CPU and 16GB, while GaussView06 was utilized for visualization [39]. The optimized structures of the free donors and acceptor molecules are aligned in parallel, reoptimized, and allowed to relax without restrictions, leading to a distinct alignment in the CTCs compared to their initial orientation. DFT provides the electronic configuration for an

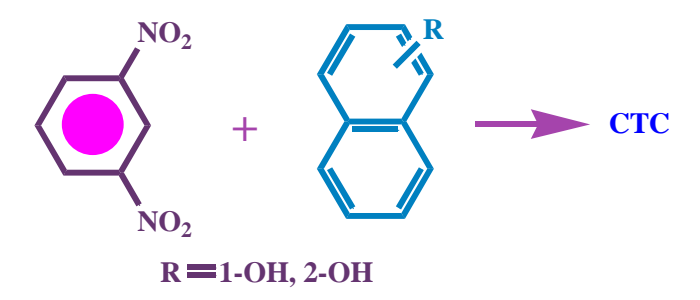
ensemble consisting of an acceptor (1, 3-dinitrobenzene) and donors (1-naphthol and 2naphthol). Energy-optimized configurations of unbound and CTCs have been examined. Full geometrical optimization was performed using DFT and Beck's three-parameter hybrid exchange functions [40] for the CTCs, via a basis set of 6-311G(d, p) [41]. The stability of the optimized structures was confirmed by frequency analysis, ensuring that all optimized structures are located at local minima on the potential energy surface. The IR frequencies determined by the "FREQ" keyword indicate that the optimized structure corresponds to a minimum on the potential energy surface. Accurate band assignments were made using animated vibrational modes in the IR spectrum. The UV spectra were obtained using the TD-DFT [42] approach. The molecular electrostatic potential (MEP) maps were generated using the same DFT level of theory. The MEP was generated using the calculated electrostatic potential due to the molecule's electron density. A grid of points in space was defined around the molecule, extending 10 Å from the molecular surface to ensure full coverage of the electrostatic environment. Natural Bond Orbital (NBO) analysis was performed to obtain atomic charges and to explore electronic delocalization. The NBO calculations were executed as follows: NBO calculations were conducted using the "POP=NBO" keyword.

Results and Discussion

Conformational Analysis of 1-Naphthol and 2-Naphthol

Hydroxyarenes play a significant role in chemistry, biology, and the life sciences, exhibiting diverse properties stemming from the hydroxy group and the aromatic π -electron system. The C-O bond in both naphthols (**1-Np** and **2-Np**) can rotate without restriction, forming two rotamers (*syn* and *anti*) for these compounds. The DFT method was employed to examine all rotamers of naphthols, and the optimized structures of these rotamers are shown in **Figure 1**. **Table 1** presents the calculated energies and structural parameters of these

rotamers using the B3LYP/6-311G (d, p) method. Regarding 1-naphthol, the *anti-1-Np* rotamer is more stable than the *syn-1-Np* rotamer based on the total energy values provided in **Table 1**. The energy difference (ΔE) for the rotamers (*anti-1-Np* and *syn-1-Np*) is -0.002523 *a.u.*, equivalent to -1.58 *kcal/mol*. The computed dipole moments for these rotamers are 1.29 and 1.40 *D*, indicating that the *anti-1-Np* rotamer is less polar. Conversely, the *syn-2-Np* rotamer is more stable than the *anti-2-Np* by 0.67 *kcal/mol*. The rotamerization process allows for to free interconversion of the rotamers, achieved through an aryl-O single bond (sigma) rotation. In *anti-*rotamers, the dihedral angle value (Φ_{OHC1C2}) is 180 degrees (coplanar state). However, in *syn-1-Np*, the rotamer Φ_{OHC1C2} value is 11 degrees, while in *syn-2-Np*, it is zero degrees. This deviation from zero in *syn-1-Np* is due to Van der Waals repulsion between the two hydrogens (OH and C1H).



Scheme 1. Synthesis reaction of two CT complexes ((1-NP)(*m*-DNB) and (2-NP)(*m*-DNB))

Table 1. Computed energy and some structural parameters for rotamers of 1-NP and 2-NP

compounds	μ (<i>D</i>)	$\Phi_{ m OHC1C2}$	$\mathbf{E}_{\mathrm{anti}}(a.u.)$	$\mathbf{E}_{\mathrm{syn}}(a.u.)$	ΔE(kcal/mol)
1-NP	μ _{anti} =1.29	$\Phi_{\text{anti}}=180$	-461.2287	-461.2262	-1.58
	$\mu_{\text{syn i}}=1.40$	$\Phi_{\mathrm{syn}i}=11$			
2-NP	μ _{anti} =1.60	$\Phi_{anti}=180$	-461.2277	-461.2288	0.67
	$\mu_{\text{syn i}}=1.06$	$\Phi_{\mathrm{syn}\mathrm{i}}$ =0			

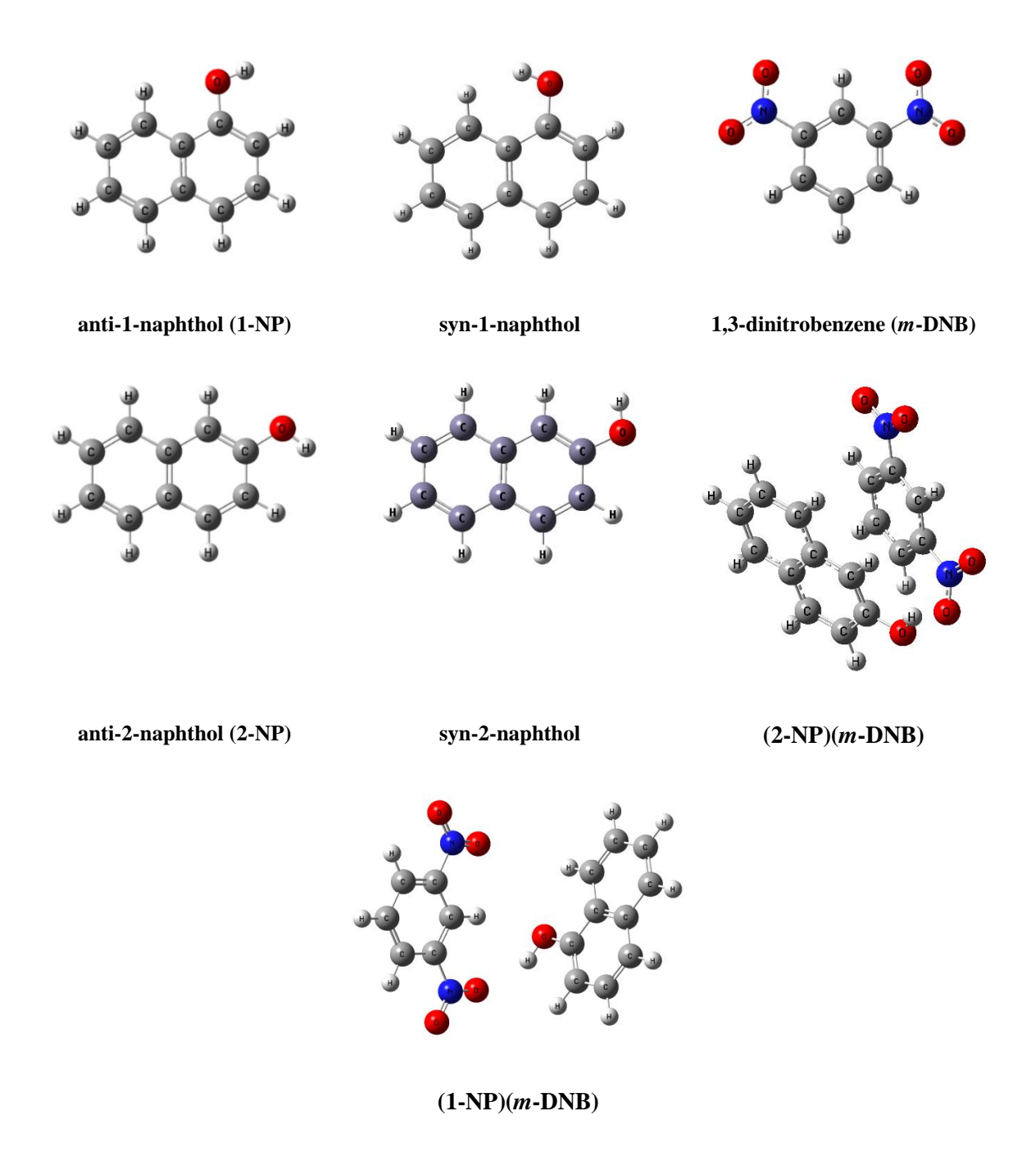


Fig. 1. Optimized geometries in the gas phase of m-DNB, 1-NP, 2-NP, and their CT complexes

Molecular Structures

The optimized structures of the free donors and acceptors are aligned in parallel, reoptimized, and allowed to relax without any restrictions. Consequently, the alignment of the two elements in the CTC is markedly distinct from their initial orientation (before the optimization process). As the donor and acceptor molecules come closer, the formation of the complex can be elucidated through CT. In both CTCs, *m*-DNB appears to interact with the π-donor (1-NP and 2-NP) molecules via the oxygen atom within the NO₂ group. It seems feasible for hydrogen bonds to form between the OH groups of naphthols and *m*-DNB. Figure 1 illustrates the optimized structures in the gas phase of the examined CTCs, free donors (1-NP, 2-NP), and the acceptor (*m*-DNB). Bond lengths selected from the optimized geometries of 1-NP, 2-NP, *m*-DNB, (1-NP)(*m*-DNB), and (2-NP)(*m*-DNB) are presented in Table 2. Δr is the bond length difference between the free molecule and the complex.

After complexation, only a small number of bond lengths remained the same, while the majority of bond lengths were modified. Certain bonds are elongated, whereas others are compressed. The highest bond elongations are found in the r_{N2-O3} bonds of the (1-NP)(m-DNB) and (2-NP)(m-DNB) complexes, showing bond length variations of 0.007 and 0.008 Å, respectively. Furthermore, during complexation, the number of bonds that become shortened surpasses elongated ones, which can be ascribed to the charge donation mechanism. The greatest bond shortenings are observed in the r_{N1-C1} bonds in the (1-NP)(m-DNB) and (2-NP)(m-DNB) complexes, with bond length variations of 0.004 and 0.006 Å, respectively. In both complexes, the r_{OH} bond is stretched by approximately 0.003 Å. It appears that hydrogen bonds are crucial in the formation of complexes.

The selected optimized bond and dihedral angles of the titled molecules in the gas phase are shown in **Table 3**. $\Delta\theta$ is the bond angle difference between the free molecule and the complex, and $\Delta \omega$ is the dihedral angle difference. These data show that bond angles are not changed, and variations in bond angle values are tiny (1 degree). But, in the case of dihedral angles, variations are large. In *m*-**DNB**, the dihedral angles (concerning the NO₂ group, $\varphi_{\text{C-C-NO}}$) are altered (about six degrees). In **1-NP** and **2-NP**, the dihedral angles (concerning the

HO group, $\phi_{\text{H-O-C-C}}$) are altered; of course, the angle alteration in (2-NP)(m-DNB) is more (about 25 degrees).

Table 2. Selected optimized bond lengths (in \mathring{A}) of **1-NP**, **2-NP**, **m-DNB**, and their CT complexes

atomic bond			bond	length		
	(1-NP)	(1-NP)(<i>m</i> -DNB)	Δr	(2-NP)	(2-NP)(<i>m</i> -DNB)	Δr
r _{C-O}	1.366	1.367	-0.001	1.367	1.366	0.001
$\mathbf{r}_{ ext{O-H}}$	0.963	0.966	-0.003	0.962	0.965	-0.003
$\mathbf{r}_{ ext{C1-C2}}$	1.377	1.378	-0.001	1.376	1.377	-0.001
r _{C2-C3}	1.413	1.413	0.000	1.417	1.419	-0.002
$\mathbf{r}_{\mathrm{C4-C10}}$	1.420	1.420	0.000	1.418	1.419	-0.001
$\mathbf{r}_{ ext{C5-C6}}$	1.374	1.374	0.000	1.373	1.374	-0.001
$ m r_{C6-C7}$	1.413	1.413	0.000	1.415	1.415	0.000
$\mathbf{r}_{ ext{C7-C8}}$	1.375	1.375	0.000	1.373	1.374	-0.001
r _{C8-C9}	1.417	1.418	-0.001	1.421	1.421	0.000
r _{C9-C1}	1.427	1.427	0.000	1.415	1.416	-0.001
	(m-DNB)			(m-DNB)		
$\mathbf{r}_{ ext{C1-C2}}$	1.387	1.388	-0.001	1.387	1.387	0.000
r _{C2-C3}	1.387	1.389	-0.002	1.387	1.386	0.001
r _{C3-C4}	1.391	1.392	-0.001	1.391	1.391	0.000
$\mathbf{r}_{\text{C4-C5}}$	1.392	1.392	0.000	1.392	1.391	0.001
$\mathbf{r}_{ ext{N1-C1}}$	1.485	1.481	0.004	1.485	1.479	0.006
$\mathbf{r}_{ ext{N2-C3}}$	1.485	1.486	-0.001	1.485	1.484	0.001

r _{N1-O1}	1.221	1.220	0.001	1.221	1.221	0.000
r_{N2-O3}	1.221	1.228	-0.007	1.221	1.229	-0.008
$r_{ m N2-O4}$	1.222	1.218	0.004	1.222	1.218	0.004

Table 3. Some optimized bond and dihedral angles (in degrees) of **1-NP**, **2-NP**, *m***-DNB**, and their CT complexes.

bond angle	(1-NP)	(1-NP)(<i>m</i> -DNB)	Δθ	(2-NP)	(2-NP)(<i>m</i> -DNB)	$\Delta \theta$
$ heta_{ ext{H-O1-C1}}$	109	110	1	-		
$\theta_{\text{O1-C1-C9}}$	116	117	1	-		
$ heta_{ ext{C8-C7-H7}}$	120	120	0	120	120	0
$ heta_{ ext{C1-C2-H2}}$	120	120	0	-		
$\theta_{\text{H-O-C2}}$	-	-	-	109	109	0
$\theta_{\text{O-C2-C1}}$	-	-	-	118	119	1
$ heta_{ ext{C2-C1-H1}}$	-	-	-	119	119	0
$ heta_{ ext{C2-C3-H3}}$	119	119	0	120	119	1
	(m-DNB)			(m-DNB)		
$\theta_{\text{N1-C1-C2}}$	119	119	0	119	118	1
$\theta_{ ext{N2-C3-C2}}$	119	119	0	119	118	1
$\theta_{ ext{N2-C3-C4}}$	119	118	1	119	119	0
$ heta_{ ext{O3-N2-O4}}$	125	124	1	125	125	0
$\theta_{\rm O1\text{-}N1\text{-}O2}$	125	126	1	125	125	0
dihedral angle	(1-NP)	(1-NP)(<i>m</i> -DNB)	Δφ	(2-NP)	(2-NP)(<i>m</i> -DNB)	Δφ

Фн2-С2-С1-О	0	0	0	-	-	
Фн-о-с1-с9	180	176	4	-	-	
Фн-0-С1-С2	0	5	5	-	-	
Фо-с1-с9-с8	0	1	1	-	-	
Фн-0-С2-С3	-	-		0	28	28
Фн-0-С2-С1	-	-		180	152	28
Фо-с2-с3-н3	-	-		0	1	1
Ф 0-С2-С1-Н1	-	-		0	1	1
	(m-DNB)			(m-DNB)		
Фс2-с1-N1-01	(m-DNB)	6	6	(m-DNB)	2	2
Фс2-С1-N1-О1 Фс2-С1-N1-О2		6 174	6		2 178	2
	0			0		
Фс2-С1-N1-О2	0 180	174	6	0 180	178	2
ФС2-С1-N1-О2 ФС4-С3-N2-О3	0 180 180	174 174	6	0 180 180	178 170	2 10
ФС2-С1-N1-О2 ФС4-С3-N2-О3 ФС4-С3-N2-О4	0 180 180 0	174 174 5	6 6 5	0 180 180 0	178 170 11	2 10 11
ФС2-С1-N1-О2 ФС4-С3-N2-О3 ФС4-С3-N2-О4 ФС6-С1-N1-О1	0 180 180 0 180	174 174 5 174	6 6 5	0 180 180 0 180	178 170 11 178	2 10 11 2

Electronic Spectrum Analysis

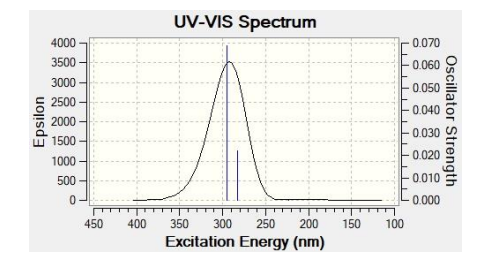
The central aspect of a CTC involves the charge transfer from a donor to an acceptor. This CT results in the creation of a specific electronic state, which is essential for comprehending the optical characteristics of the compound. The electronic structure of a CTC is the main factor in determining its optical properties. When a CTC is exposed to electromagnetic

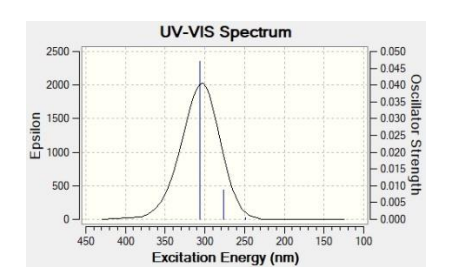
radiation, it shows unique absorption and emission traits commonly utilized to study complex properties. The absorption spectrum of CTC commonly displays specific bands that represent the transitions from the complex's ground state to its higher energy states. These changes appear as absorbance peaks in UV-Vis spectra and are influenced by factors like solvent polarity, temperature, and kinds of donor and acceptor molecules [43].

The TD-DFT method was employed to determine the absorption maxima wavenumber (λ_{max}) . Figure 2 and Table 4 show the electronic absorption spectra of m-dinitrobenzene, 1-naphthol, 2-naphthol, and their complexes within the UV-Visible range of 200 to 700 nm. The establishment of CTC formation is evidenced by the newly observed absorption maxima bands (CT band). In the cases of (1-NP)(m-DNB) and (2-NP)(m-DNB) complexes, the CT bands are observed at 638 nm and 603 nm, respectively, which do not appear in the UV-Vis spectra of the separate donor and acceptor. The CTC absorptions are displaced to a longer wavelength of approximately 300 nm. Mulliken identifies the decreased energy absorption seen in the donor-acceptor integrated system, which is a characteristic aspect of the $\pi-\pi^*$ CT interaction (π HOMOD- π^* LUMOA). This alteration leads to an increased π -electron density in the acceptor molecule and a decrease in the donor.

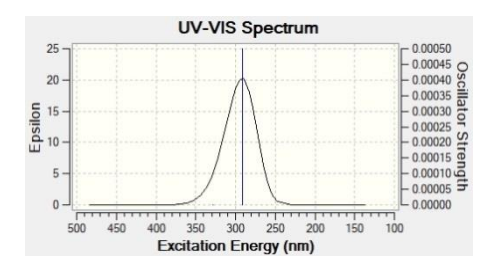
Table 4. Calculated maximum absorption wavelengths (λ_{max} , nm) of donors (1-NP and 2-NP), acceptor (m-DNB), and their complexes in the gas phase.

	$\lambda_{\max}(nm)$	$\lambda_{\max}(nm)$
Compound	computational	experimental
(1-NP)	300	245, 335
(2-NP)	306	285, 328
(m-DNB)	328	340
(1-NP)(<i>m</i> -DNB)	638	-
(2-NP)(m-DNB)	603	-

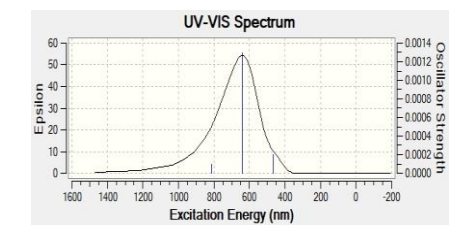




(a) Simulated UV-visible spectrum of (1-NP)

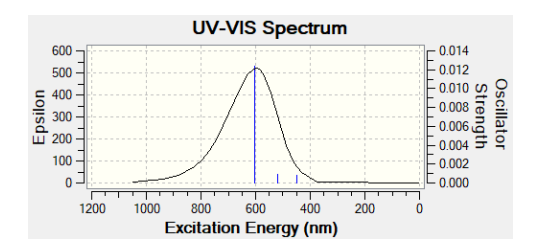


(b) Simulated UV-visible spectrum of (2-NP)



(c) Simulated UV-visible spectrum of (*m*-**DNB**)

(d) Simulated UV-visible spectrum of (1-NP)(*m*-DNB)



(e) Simulated UV-Visible spectrum of (2-NP)(m-DNB)

Fig. 2. Simulated electronic absorption spectra of two CT complexes and their reactants in the gas phase

Infrared (IR) Spectrum Analysis

Vibrational spectroscopy is an important method for studying CTCs, offering qualitative and quantitative insights into their formation, stability, and the interactions between donor and acceptor. The vibrational spectrum can provide information about the interactions between the donor and an acceptor, such as hydrogen bonding or π - π stacking, which are central to the stability of the CTC. This method can aid in detecting the existence of CTCs by observing specific spectral features that arise from the interactions between the donor and acceptor molecules. The formation of a CTC often leads to shifts in vibrational frequencies due to changes in the electronic environment and molecular geometry.

The infrared absorption spectra were computed for 1-NP, 2-NP, *m*-DNB, and their corresponding complexes. The summarized IR wavenumbers and their assignments for these compounds are presented in **Table 5.** The number of vibrational modes for non-linear molecules is derived from the 3N-6 equation, yielding vibrational mode numbers 51, 51, 42, and 99 for 1-NP, 2-NP, *m*-DNB, and the two complexes, respectively. Certainly, following molecular spectroscopy, each complex should have wavenumbers of 93; however, the calculations indicate 99 vibrational modes for these complexes.

The IR spectrum of (1-NP)(*m*-DNB) complex compared to the simple component reveals an apparent shift of the CH stretching vibration modes of the acceptor to lower wavenumbers

(3197, 3227, 3229, 3247 cm^{-1} in **m-DNB** and 3223, 3227, 3230, 3198 cm^{-1} in complex). In contrast, the donors are shifted to higher values (3148, 3158, 3167, 3171, 3183, 3186, and 3205 cm⁻¹ in **1-NP** and 3185, 3184, 3171, 3168, 3159, 3158, 3209 cm⁻¹ in (**1-NP**)(m-DNB) complex). The NO₂ bands of the acceptor at 1368 cm⁻¹ (unsymmetrical stretching), 1377 cm⁻¹ (symmetrical stretching) in m-DNB, and at 1375 cm⁻¹ (unsymmetrical stretching) and 1387 cm⁻¹ (symmetrical stretching) in the complex, exhibit some interesting changes. This behavior signifies a greater differentiation of the energy states of the NO₂ group in the CTC compared to the free acceptor. The spectra of the free acceptors show the asymmetric NO₂ bands as two neighboring peaks. The lower energy bands exhibit a shift to reduced wavenumber, signifying enhanced polarization of the NO₂ groups associated with these bands, resulting from the heightened electron density on the acceptor's ring. The asymmetrical NO₂ band of the CT complexes with the acceptor (like m-nitrobenzene) displays a shift to a lower wavenumber, indicating that $n-\pi^*$ interaction should be ruled out [44]. The calculated O-H for the free **1-NP** and **2-NP** appeared in 3833.9 and 3837 cm⁻¹, respectively. These wave numbers in complexes are 3779 and 3804 cm⁻¹. The calculated C=Cs are 1368 cm^{-1} for **m-DNB** and 1554, 1620, 1641, and 1672 cm^{-1} for **1-NP**. These peaks in the (1-NP)(m-DNB) complex appeared in 1467, 1499 cm⁻¹ (stretching vibration in m-**DNB**), and 1040, 1389, 1410, 1434 cm^{-1} (stretching vibration in **1-NP**). Typically, the IR bands of the acceptor molecules were displaced to lower frequencies, while the IR bands of the donor molecules were shifted to higher frequencies in their corresponding complexes.

Thermodynamic Parameters

Understanding CTC formation and stability relies heavily on their interaction with thermodynamic parameters. These parameters typically include: **Gibbs free energy change** (ΔG , the spontaneity of CT process), **Enthalpy change** (ΔH , the heat absorbed or released during the complex formation), **Entropy change** (ΔS , the change in randomness during the

creation of the complex), and **interaction energy** (ΔE , which aids in comprehending the types of interactions (ionic, covalent, van der Waals, *etc.*)). Furthermore, it is essential to consider the importance of temperature and solvent effects on these thermodynamic parameters for practical applications. Temperature fluctuations can affect the kinetic and thermodynamic stability of CTCs, whereas the solvent's polarity can impact the rates of CT and the formation of these complexes [45].

Concerning data in output files, values of ΔE_{int} , ΔH_{int} , ΔS_{int} , and ΔG_{int} for these complexes were obtained computationally at a temperature of 25°C and a pressure of 1 atm. (see **Table 6**). The ΔG_{int} values for (1-NP)(m-DNB) and (2-NP)(m-DNB) complexes are 4.383 and 9.354 kcal/mol, respectively. The positive values indicate that the formation of the complexes is not thermodynamically favorable. Of course, forming (1-NP)(m-DNB) is more favorable than forming another complex. The interaction enthalpy (ΔH_{int}) values for both complexes are negative, indicating that the formation of the complexes releases heat. Additionally, negative values of interaction entropies (ΔS_{int}) propose a reduction in randomness, while stronger interactions typically result in more stable complexes as indicated by interaction energy (ΔE_{int}).

Table 6. Calculated ΔE_{int} , ΔH_{int} , ΔS_{int} , and ΔG_{int} for (1-NP)(m-DNB) and (2-NP)(m-DNB) complexes

complex	$\Delta \mathrm{E}_{\mathrm{int}}$	ΔH_{int}	ΔS_{int}	ΔG_{int}
	(kcal/mol)	(kcal/mol)	(kcal/K.mol)	(kcal/mol)
(1-NP)(<i>m</i> -DNB)	-3.29	-3.88	-0.03	4.38
(2-NP)(<i>m</i> -DNB)	-1.36	-1.95	-0.04	9.35

Dipole Moment and Polarizability Analysis

The ground state dipole moment (μ), **average** polarizability (α_{ave}), and first hyperpolarizability (β_{total}) for (**1-NP**), (*m***-DNB**), (**2-NP**), (**1-NP**)(*m***-DNB**), (**2-NP**)(*m***-DNB**), and urea (as a standard compound in NLO materials) were calculated via Gaussian software (see **Table 7**).

The ground state dipole moment of a molecule quantifies the distribution of positive and negative charges within the molecule when it is at its lowest energy state. It is a vector quantity, characterized by both magnitude and direction, and is vital for understanding molecular interactions and predicting the behavior of the CTC in various environments [46]. The formation of a CTC typically leads to an alteration in the dipole moment compared to the individual component molecules. This alteration reflects the strength and character of the interaction. A notable dipole moment can enhance the stability of CTC via dipole-dipole interactions. This stability is urgent for CTC applications in organic photovoltaics and other electronic devices. Also, it can be considered a driving force for CTC formation. CTC's high dipole moment values were found from its electronic and nuclear contributions and were calculated to be 5.23 and 57 *D* for (1-NP)(*m*-DNB) and (2-NP)(*m*-DNB) complexes, respectively.

Average polarizability (α_{ave}) refers to the measure of how easily an external electric field can distort the electron cloud of a molecule. Polarizability measures the linear optical response and sets the stage for higher-order responses. In NLO materials, high polarizability can enhance the efficiency of processes like second-harmonic generation and electro-optic switching. Understanding polarizability helps in selecting materials with suitable optical properties for specific applications. Materials with large polarizability are preferred for devices that require a significant change in refractive index with an applied field. The

polarizability of a material is also influenced by its crystal symmetry, which determines its ability to exhibit NLO effects. A CTC can exhibit NLO properties due to its unique electronic structure and CT mechanism between the components of the CTC. Thus, the study of the optical properties of CTCs not only provides insights into their electronic engagements but also paves the way for applications in organic electronics, photonics, and sensor technologies. The average polarizability of a CTC can be influenced by the nature of the donor and acceptor, the distance between them, and the solvent environment [47]. **Table 7** shows donors (1-NP and 2-NP), acceptor (m-DNB), and two resulting in CTC have more α_{ave} values than urea, also (1-NP)(m-DNB) and (2-NP)(m-DNB) have bigger polarizability than their components.

Hyperpolarizability characterizes the second-order (nonlinear) response of a material to an electric field. It allows for the description of phenomena like second-harmonic generation and self-focusing. A material with a high hyperpolarizability can produce strong NLO effects, which are essential for many advanced optical applications. The first hyperpolarizability (β_{total}) is critical in understanding and predicting multi-photon absorption processes, where multiple photons are absorbed simultaneously. It is vital for applications such as laser technologies and imaging. β_{total} of a molecule is an important parameter indicating its NLO response. For a CTC, hyperpolarizability can be significantly enhanced if a significant variation exists in the electron affinity and ionization potential of components [48]. The extent of CTC upon excitation can contribute to larger values of hyperpolarizability. The following equation (Eq. 1) was used to calculate the studied molecules' first-order hyperpolarizability (β_{total}).

$$\beta_{total} = [(\beta_{xxx} + \beta_{xyy} + \beta_{xzz})^2 + (\beta_{yyy} + \beta_{yzz} + \beta_{yxx})^2 + (\beta_{zzz} + \beta_{zyy} + \beta_{zxx})^2]^{1/2}$$
Eq. (1)

The energy gap of frontier orbitals assists in defining the chemical reactivity, charge delocalization, photophysical characteristics, and kinetic stability of the molecule [49-52]. At

the core of the study of CTCs is the concept of FMO orbitals. A CTC with a narrow energy gap exhibits increased polarizability, is typically associated with heightened chemical reactivity and reduced kinetic stability, and is often referred to as a soft molecule. A diminished energy gap enables simpler electron transfer, making the complex more stable. When excited, the electron can be raised from the donor's HOMO to the acceptor's LUMO, resulting in a charge-separated state. This phenomenon is crucial in light-harvesting systems, where effective charge separation can enhance energy conversion processes. Moreover, the type of CT, whether intramolecular or intermolecular, affects the distribution of electron density and the resulting spectral characteristics.

Table 7. Calculated ground state dipole moment (Debye, D), average polarizability (α_{ave}), first hyperpolarizability (β_{total}), and frontier molecular orbitals energies for urea, (1-NP), (m-DNB), (2-NP), and the two studied complexes

compound	(T))	α_{ave}	a_{ave}	β_{total}	β_{total}	$\mathbf{E}_{\mathbf{LUMO}}$	$\mathbf{E}_{\mathbf{HOMO}}$	$\Delta \mathbf{E_t}$
	μ (<i>D</i>)	(au)	(esu)	(au)	(esu)	(eV)	(eV)	(eV)
1-NP	1.29	110.45	16.37×10 ⁻²⁴	194.93	1.68×10 ⁻³⁰	-1.07	-5.69	4.62
2-NP	1.59	112.00	16.61×10 ⁻²⁴	389.32	3.36×10^{-30}	-1.21	-5.75	4.53
m-DNB	4.2	90.27	13.38×10 ⁻²⁴	366.08	3.16×10^{-30}	-3.32	-8.62	5.30
(1-NP)(m-DNB)	5.23	202.47	30.01×10 ⁻²⁴	645.91	5.58×10^{-30}	-3.54	-5.57	2.03
(2-NP)(m-DNB)	5.17	193.75	28.71×10 ⁻²⁴	1626.97	14.06×10 ⁻³⁰	-3.66	-6.72	3.06
urea	3.62	28.00	4.15×10 ⁻²⁴	69.95	0.60×10^{-30}	-0.63	-7.04	5.79

The calculated HOMO and LUMO plots for (1-NP)(*m*-DNB), (2-NP)(*m*-DNB), 1-NP, 2-NP, and *m*-DNB were displayed in Figure 3. The distribution pattern of electron density in the examined molecules can be observed from their HOMO and LUMO orbitals. In CTCs, the HOMO was confined solely to 1-NP and 2-NP (acting as donors), while the LUMO was exclusively localized on *m*-DNB (acting as the acceptor) in a reversed manner. Each HOMO

and LUMO features nodes that are symmetrically arranged within each HOMO and LUMO. The surface contour of FMOs reflects molecular dimensions and shape, along with the electrostatic potential level. The calculated energies of FMOs (E_{HOMO} and E_{LUMO}) and the energy gaps (ΔE_t) for the specified molecules are presented in **Table 7**. From **Table 7**, it is noteworthy that the LUMO energy levels of the CTCs (-3.54, -3.66 eV) are similar to those of m-DNB (-3.32 eV), while the HOMO energy levels of the CTCs (-5.57, -6.72 eV) are approximately aligned with those of 1-NP and 2-NP (-5.69, -5.75 eV). This inclination for the localization of FMOs in CTCs closely resembles the previously documented electron donoracceptor systems [53]. A more negative E_{HOMO} means harder to oxidize; a more negative E_{LUMO} means harder to reduce. The ΔE_t is a crude proxy for chemical reactivity: smaller gaps often correlate with higher reactivity and lower kinetic/thermodynamic stability in many environments. Energy gap between the highest occupied molecular orbital (HOMO) and the lowest unoccupied molecular orbital (LUMO) of the complex, i.e., $\Delta E_t = E_{LUMO} - E_{HOMO}$. In many contexts, a larger ΔE_t corresponds to greater electronic stability (less reactivity) and a smaller ΔE_t indicates higher reactivity. The smaller frontier orbital gap values in CTCs (2.03, 3.06 eV) render them more reactive and less stable. The (1-NP)(m-DNB) complex possesses a smaller energy gap compared to the others, suggesting that the (1-NP)(m-DNB) complex is more reactive and that its electron density can vary more readily.

In literary works, comparable values of ΔE_t have been noted. The energy gap between HOMO and LUMO for the [(β -cyclodextrin)(DDQ)] and [(β -cyclodextrin)(TCNE)] complexes is -2.694 eV and -2.294 eV, respectively [54]. The value of ΔE_t is 2.61 eV for the CTC obtained from 4-dimethylaminopyridine and DDQ [55]. In the investigation of interactions between 1-hydroxypyrene (PyOH) and aromatic amino acids (Phe, Tyr, and Trp), energy gap values were found to be 3.77, 3.73, and 3.71 eV for the complexes PyOH-Phe, PyOH-Tyr, and PyOH-Trp, respectively [56].

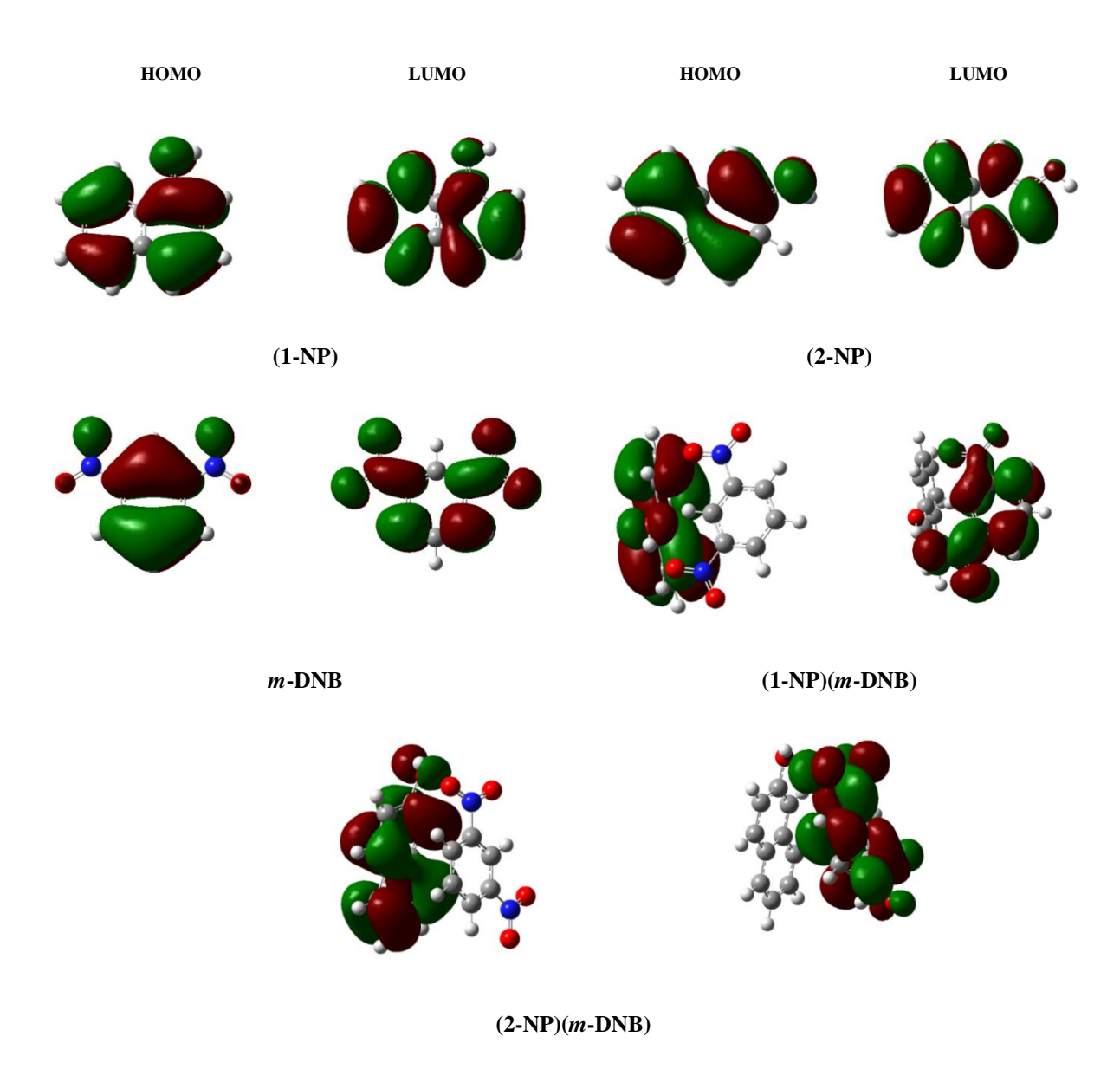


Fig. 3. Calculated diagrams of FMOs for 1-NP, 2-NP, m-DNB, (1-NP)(m-DNB), and (2-NP)(m-DNB)

Natural Bonding Orbital

Natural bonding orbital analysis (NBO) is a computational method used to analyze the bonding in molecules based on quantum chemistry [57]. NBO provides insights into the electronic structure of molecules by identifying the 'natural' orbitals that electrons occupy. NBOs are the orbitals that correspond to the largest probability density for finding an electron. These orbitals offer a clear picture of how electrons are distributed in a molecular system. By examining the electron density in NBOs, one can identify regions of electron donation or acceptance, which is particularly relevant in CTCs. NBO analysis allows for a

detailed examination of donor-acceptor interactions, providing energy donated from one NBO to another, which can be decisive for understanding CT [58, 59]. Also, it can offer significant understanding regarding the characteristics and stability of CTCs by elucidating the electronic structure and interactions present in these complexes. NBO analysis allows researchers to visualize the electron density and assess how it shifts during the chargetransfer process. Electron density localization on the donor or acceptor increases the likelihood of effective overlap between the orbitals involved in the transfer, thereby enhancing charge-transfer efficiency. A significant factor influencing charge transfer is the energy difference between the HOMO of the donor and the LUMO of the acceptor. Effective charge transfer requires proper alignment and overlap of these orbitals. A shift in electron density that optimizes the spatial arrangement can significantly improve orbital overlap, thus increasing the rate of CT. The strength of the interaction between the donor and acceptor is influenced by the degree of electron density overlap. Greater shifts in electron density that lead to high overlap between the donor's HOMO and the acceptor's LUMO enhance the likelihood of efficient charge transfer. The stabilization of the charge-transfer complex through π - π stacking or dipole-dipole interactions can be understood through NBO analysis. Effective electron density shifts contribute to the overall stabilization of the charge-transfer state, which is critical for sustaining charge separation following the transfer. The movement of electron density is not static; it can be dynamic and subject to molecular vibrations and solvent effects. NBO can provide insights into how these shifts evolve and their correlation with changes in charge-transfer rates.

Table 8. Calculated NBO atomic charges of (1-NP)(m-DNB) complex and its free components

atom	charge/free	charge/complex	∆charge
1	-NP		
C1	0.368	0.363	0.006
C2	-0.300	-0.299	-0.001
C3	-0.078	-0.080	-0.002
C4	-0.211	-0.212	0.001
C5	-0.079	-0.081	-0.002
C6	-0.093	-0.094	0.001
C7	-0.200	-0.200	0.000
C8	-0.071	-0.072	0.001
C9	-0.002	-0.003	0.001
C10	-0.040	-0.041	-0.001
O	-0.675	-0.700	-0.025
ОН	0.465	0.488	0.023
<i>m</i> -	DNB		
C1	0.069	0.066	-0.003
C2	-0.075	-0.075	0.000
C3	0.069	0.072	-0.003
C4	-0.058	-0.053	0.005
C5	-0.081	-0.081	0.000
C6	-0.058	-0.056	0.002

N1	0.517	0.527	0.010
N2	0.517	0.518	0.001
01	-0.367	-0.420	-0.053
O2	-0.374	-0.353	0.021
О3	-0.367	-0.363	-0.004
O4	-0.374	-0.374	0.000

In *m*-DNB, the proton is moved to the O2 atom by slightly reducing its negative atomic charge to -0.353e from -0.374e of the free acceptor. The significant charge presence on O = -0.700e of **1-NP** in complex indicates the presence of O···H···O type interaction in this complex, with other atoms like OH (0.488e from 0.465e) and O1 (-0.4200e from -0.367e) also exhibiting NBO charge shifts from the free donor and acceptor in [(**1-NP**)(**m-DNB**)]. These changes offer solid evidence of the interaction between **1-NP** and *m-DNB*, as shown in **Table 8**, involving the (**1-NP**)(**m-DNB**) complex and proton transfer.

Table 9. Calculated NBO atomic charges of (2-NP)(m-DNB) complex and its free components

atom	charge/free	charge/complex	Δcharge
2	2-NP		
C1	-0.250	-0.251	-0.001
C2	0.340	0.329	0.011
C3	-0.272	-0.263	0.009
C4	-0.056	-0.064	-0.008
C5	-0.071	-0.075	-0.001

C7 -0.091 -0.091 0.000 C8 -0.085 -0.085 0.000 C9 -0.035 -0.040 -0.005 C10 -0.077 -0.077 0.000 O -0.668 -0.680 -0.012 OH 0.460 0.206 0.254	C6	-0.210	-0.209	0.010
C9 -0.035 -0.040 -0.005 C10 -0.077 -0.077 0.000 O -0.668 -0.680 -0.012 OH 0.460 0.206 0.254 m-DNB C1 0.069 0.071 -0.002 C2 -0.075 -0.067 0.008 C3 0.069 0.073 -0.004 C4 -0.058 -0.053 0.005 C5 -0.081 -0.080 0.001 C6 -0.058 -0.053 0.005 N1 0.517 0.522 0.005 N2 0.517 0.518 0.001 O1 -0.367 -0.349 -0.018 O2 -0.374 -0.414 0.040 O3 -0.367 -0.370 0.003	C7	-0.091	-0.091	0.000
C10 -0.077 -0.077 0.000 O -0.668 -0.680 -0.012 OH 0.460 0.206 0.254 m-DNB C1 0.069 0.071 -0.002 C2 -0.075 -0.067 0.008 C3 0.069 0.073 -0.004 C4 -0.058 -0.053 0.005 C5 -0.081 -0.080 0.001 C6 -0.058 -0.053 0.005 N1 0.517 0.522 0.005 N2 0.517 0.518 0.001 O1 -0.367 -0.349 -0.018 O2 -0.374 -0.414 0.040 O3 -0.367 -0.370 0.003	C8	-0.085	-0.085	0.000
O -0.668 -0.680 -0.012 OH 0.460 0.206 0.254 m-DNB C1 0.069 0.071 -0.002 C2 -0.075 -0.067 0.008 C3 0.069 0.073 -0.004 C4 -0.058 -0.053 0.005 C5 -0.081 -0.080 0.001 C6 -0.058 -0.053 0.005 N1 0.517 0.522 0.005 N2 0.517 0.518 0.001 O1 -0.367 -0.349 -0.018 O2 -0.374 -0.414 0.040 O3 -0.367 -0.370 0.003	C9	-0.035	-0.040	-0.005
OH 0.460 0.206 0.254 m-DNB C1 0.069 0.071 -0.002 C2 -0.075 -0.067 0.008 C3 0.069 0.073 -0.004 C4 -0.058 -0.053 0.005 C5 -0.081 -0.080 0.001 C6 -0.058 -0.053 0.005 N1 0.517 0.522 0.005 N2 0.517 0.518 0.001 O1 -0.367 -0.349 -0.018 O2 -0.374 -0.414 0.040 O3 -0.367 -0.370 0.003	C10	-0.077	-0.077	0.000
m-DNB C1 0.069 0.071 -0.002 C2 -0.075 -0.067 0.008 C3 0.069 0.073 -0.004 C4 -0.058 -0.053 0.005 C5 -0.081 -0.080 0.001 C6 -0.058 -0.053 0.005 N1 0.517 0.522 0.005 N2 0.517 0.518 0.001 O1 -0.367 -0.349 -0.018 O2 -0.374 -0.414 0.040 O3 -0.367 -0.370 0.003	0	-0.668	-0.680	-0.012
C1 0.069 0.071 -0.002 C2 -0.075 -0.067 0.008 C3 0.069 0.073 -0.004 C4 -0.058 -0.053 0.005 C5 -0.081 -0.080 0.001 C6 -0.058 -0.053 0.005 N1 0.517 0.522 0.005 N2 0.517 0.518 0.001 O1 -0.367 -0.349 -0.018 O2 -0.374 -0.414 0.040 O3 -0.367 -0.370 0.003	ОН	0.460	0.206	0.254
C2 -0.075 -0.067 0.008 C3 0.069 0.073 -0.004 C4 -0.058 -0.053 0.005 C5 -0.081 -0.080 0.001 C6 -0.058 -0.053 0.005 N1 0.517 0.522 0.005 N2 0.517 0.518 0.001 O1 -0.367 -0.349 -0.018 O2 -0.374 -0.414 0.040 O3 -0.367 -0.370 0.003	m-I	ONB		
C3 0.069 0.073 -0.004 C4 -0.058 -0.053 0.005 C5 -0.081 -0.080 0.001 C6 -0.058 -0.053 0.005 N1 0.517 0.522 0.005 N2 0.517 0.518 0.001 O1 -0.367 -0.349 -0.018 O2 -0.374 -0.414 0.040 O3 -0.367 -0.370 0.003	C1	0.069	0.071	-0.002
C4 -0.058 -0.053 0.005 C5 -0.081 -0.080 0.001 C6 -0.058 -0.053 0.005 N1 0.517 0.522 0.005 N2 0.517 0.518 0.001 O1 -0.367 -0.349 -0.018 O2 -0.374 -0.414 0.040 O3 -0.367 -0.370 0.003	C2	-0.075	-0.067	0.008
C5 -0.081 -0.080 0.001 C6 -0.058 -0.053 0.005 N1 0.517 0.522 0.005 N2 0.517 0.518 0.001 O1 -0.367 -0.349 -0.018 O2 -0.374 -0.414 0.040 O3 -0.367 -0.370 0.003	C3	0.069	0.073	-0.004
C6 -0.058 -0.053 0.005 N1 0.517 0.522 0.005 N2 0.517 0.518 0.001 O1 -0.367 -0.349 -0.018 O2 -0.374 -0.414 0.040 O3 -0.367 -0.370 0.003	C4	-0.058	-0.053	0.005
N1 0.517 0.522 0.005 N2 0.517 0.518 0.001 O1 -0.367 -0.349 -0.018 O2 -0.374 -0.414 0.040 O3 -0.367 -0.370 0.003	C5	-0.081	-0.080	0.001
N2 0.517 0.518 0.001 O1 -0.367 -0.349 -0.018 O2 -0.374 -0.414 0.040 O3 -0.367 -0.370 0.003	C6	-0.058	-0.053	0.005
O1 -0.367 -0.349 -0.018 O2 -0.374 -0.414 0.040 O3 -0.367 -0.370 0.003	N1	0.517	0.522	0.005
O2 -0.374 -0.414 0.040 O3 -0.367 -0.370 0.003	N2	0.517	0.518	0.001
O3 -0.367 -0.370 0.003	O1	-0.367	-0.349	-0.018
	O2	-0.374	-0.414	0.040
O4 -0.374 -0.374 0.000	О3	-0.367	-0.370	0.003
	O4	-0.374	-0.374	0.000

In *m*-DNB, the proton is transferred to the O1 atom by slightly decreasing its negative atomic charge to -0.349e from the -0.367e of the unbound acceptor. The significant presence of charge on O (-0.680e) of **2-NP** in the complex indicates the occurrence of an O··H··O type interaction in this system. Additional atoms of (**2-NP**)(*m*-DNB), such as OH (0.206e from 0.460e) and O2 (-0.414e from -0.374e), also display a shift in NBO charges from the free donor and acceptor. These changes provide significant support for the (**2-NP**)(*m*-DNB) complex and the proton transfer interaction occurring between **2-NP** and *m*-DNB, as detailed in **Table 9**.

Molecular Electrostatic Potential (MEP)

A MEP denotes the electrostatic potential created by the distribution of a molecule's electrons. It explains how a molecule engages with other molecules, ions, or substrates. It illustrates how the electron cloud of a molecule can affect adjacent charged entities. The MEP maps serve to depict areas of variable charge within a molecule, and they are represented as a color-coded surface enveloping the molecule, with regions of significant negativity (electron-rich sections) typically displayed in red and positivity (electron-deficient regions) in blue. Grasping the MEP is crucial for forecasting reactivity, intermolecular interactions, and the arrangement of various molecules within complexes. The MEP maps serve as the most useful electrostatic property for examining the connection between a molecule's structure and its activity; this illustrates the interaction energy resulting from the electrical charges produced by the molecule's electrons and nuclei [60, 61].

The MEPs of the donor and acceptor molecules can assist in forecasting the viability of CT. A positive electrostatic interaction between the donor's electron-dense areas and the acceptor's electron-deficient areas frequently aids in creating a CTC. The properties of the MEP can additionally affect the stability and traits of the resulting CTC, aiding in the creation of new materials or functions in supramolecular chemistry. A MEP provides information on

the electron distribution and reactivity of molecules, which is essential for anticipating and comprehending the creation of CTCs.

The MEPs of both complexes were calculated using the same theoretical level applied in the geometry optimization (refer to **Figure 4**). Notable alterations have been observed for the complex moiety concerning naphthols or **m-DNB**, validating the CT pathway. As illustrated in **Figure 4**, the MEP diagram of **m-DNB** exhibited a positive area (blue) focused at the center of the phenyl ring, and negative potential regions were noted near the nitrogen atoms of the NO₂ groups. In the **1-NP**, the negative potential (-0.041 au) is primarily linked to the center of the benzene rings due to p-electrons and the donation of lone pair electrons from the hydroxyl group. A positive potential (0.038 au) was found on the O atom of the hydroxyl group, where 1-NP interacts with m-DNB; the central positive value of m-DNB reduced to 0.0204 au, while the N atom and O atom of the group potential rose to -0.052 and -0.041 au, respectively. The potential at the center of the benzene ring lowered to 0.0095 au, while the N atom of the hydroxyl group in 1-NP potential (0.066 au) increased due to the CT interaction. The n-electrons move from the oxygen atom of 1-NP to the N=O groups in m-DNB. These findings further support the notion that **m-DNB** is regarded as an effective electron acceptor in forming CT complexes with various donors [62, 63]. Based on the discussions, it is evident that the energy of orbital interaction primarily arises from the CT between filled and vacant orbitals. The MEPs will aid in establishing the relative orientation of the donor and acceptor molecules in forming the CT complex.

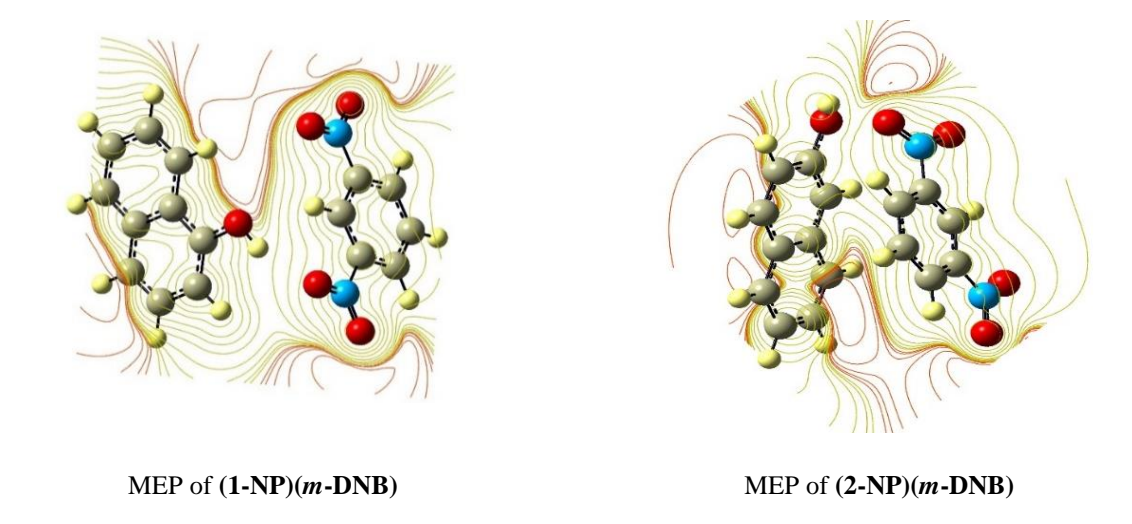


Fig. 4. Calculated molecular electrostatic potential maps for (1-NP)(*m*-DNB) and (2-NP)(*m*-DNB) complexes in the ground state.

Conclusions

The conformational analysis of naphthols (1-NP and 2-NP) identified two rotamers (syn and anti) for both 1-naphthol and 2-naphthol, with low energy gap differences (1.58 and 0.67 kcal/mol), and are quickly converted to each other at room temperature. Structural comparison of CTCs with free components showed alterations in bond lengths and indicated hydrogen bond formations. The complex formation is explained through CT as m-DNB interacts with the π -donor (1-NP and 2-NP) molecules via the oxygen atom within the NO₂ group. The feasibility of hydrogen bonds forming between the OH groups of naphthols is observed. Significant bond elongations are noted in specific bonds of the complexes, while several bonds undergo shortening, indicating a charge donation mechanism. The data displaying optimized bond and dihedral angles of the molecules in the gas phase reveal minimal changes in bond angles with very slight variations. For both complexes, there is no significant alteration in the naphthols bond lengths, but the changes near the OH group are seen (enlargement of 0.003 \mathring{A} , indicative hydrogen bond between OH and NO₂). The acceptor part alterations are more (increasing $r_{\rm NO}$ by 0.007 \mathring{A} and decreasing $r_{\rm CN}$ by about 0.005 \mathring{A}) as

an indication of hydrogen bond formation. Dihedral angle values in the OH and NO₂ regions (3-28 degrees) are more concerning.

UV-Vis analysis unveiled new absorption bands at 638 nm and 603 nm (CT bands) in the CTCs, reflecting electronic transitions. IR analysis revealed 99 vibrational frequencies in the complexes, with IR band shifts correlated to the CT interaction properties. Ninety-nine were not derived from the 3N-6 equation; the six vibrational modes in the analyzed complexes relate to the simultaneous vibrations of both the donor and the acceptor. Thermodynamic variables, including interaction energy, enthalpy, entropy, and Gibbs free energy, suggest that the complexes are not very stable and their creation is non-spontaneous and exothermic. The interaction energy values (-0.293 and -1.359 kcal/mol) indicate that there is no significant interaction between the donor and the acceptor, as CTCs are created through weak intermolecular forces. The HOMO orbitals are spread across the donor molecules, whereas the LUMO orbitals are found on the acceptor molecules, validating the CT process. The dipole moments, mean polarizability, and first static hyperpolarizability indicate notable charge separation in the complexes, suggesting possibilities for nonlinear optical applications. High dipole moments enhance CTC stability via dipole-dipole interactions. For two complexes, the hyperpolarizability values (β_{total}) are 5.58×10^{-30} and 14.06×10^{-30} esu, which are approximately 9 to 23 times greater than that of urea. The NBO and MEP analyses illustrate the electron density distribution and verify the electrostatic interactions between the donor and acceptor molecules. Notable alterations in the CT pathway have been observed in the complex moiety involving naphthols or 1,3-dinitrobenzene (m-DNB), validating the CT process. Future research on charge transfer complexes involving naphthol and dinitrobenzene could advance fundamental chemistry and practical applications significantly. By addressing these gaps, future research can enhance the understanding of charge transfer complexes involving naphthol and dinitrobenzene.

References

- [1] Mulliken, R.S. Structures of a complex formed by halogen molecules with aromatic and oxygenated solvents. Journal of the American Chemical Society, 72 (1950) 600-608. https://doi.org/10021/ja01157a151.
- [2] Alsanie, W. F., et al. Increasing the Efficacy of Seproxetine as an Antidepressant Using Charge–Transfer Complexes. Molecule, 27 (2022) 3290. https://doi.org/10.3390/molecules27103290.
- [3] Darwish, I. A., Darwish, H. W., Ali A. M., Almutairi, H. S. Spectrophotometric Investigations of Charge-transfer Complexes of Tyrosine Kinase Inhibitors with Iodine as a π -Electron Acceptor: Application to Development of Universal High-Throughput Microwell Assay for Their Determination in Pharmaceutical Formulations. Medicina, 59 (2023) 775. https://doi.org/10.3390/medicina59040775.
- [4] Murata, T., et al. Hydrogen-Bond Interaction in Organic Conductors: Redox Activation, Molecular Recognition, Structural Regulation, and Proton Transfer in Donor–Acceptor Charge-Transfer Complexes of TTF-Imidazole. Journal of the American Chemical Society, 129 (2007) 10837–10846. https://doi.org/10021/ja072607m
- [5] Rezvan, V. H., Salehzadeh, J. Exploring Charge Transfer Complexes of Fluoroquinolone Drugs and π -Acceptors (Picric Acid and 3,5-Dinitrobenzoic Acid): DFT Insights Into Electronic Interactions, Thermodynamic Stability, FMOs, and NLO Properties. ChemistrySelect, 10 (2025) e202405137. https://doi.org/10002/slct.202405137
- [6] Rezvan, V. H., DFT study of Molecular structure and optical properties of charge-transfer complexes derived from Tetrathiafulualene and Tetracyanoquinodimethane derivatives. Journal of Chemical Reactivity and Synthesis, 11 (2021) 6-11.

- [7] Beigloo, N. A. B., Rezvan, V. H., Ebrahimzadeh-Rajaei, Gh., Shamel, A. New Charge Transfer Complex between Melamine and 4-Nitrobenzoic Acid: Synthesis, Spectroscopic Characterization, and DFT Studies. Journal of Molecular Structure, 1322 (2024) 140469. https://doi.org/10016/j.molstruc.202440469.
- [8] Khan, I. M., Alam, K, Alam, M. J., Ahmad, M. Spectrophotometric and photocatalytic studies of H-bonded charge-transfer complex of oxalic acid with imidazole: Single crystal XRD, experimental and DFT/TD-DFT studies. New Journal of Chemistry, 43 (2019) 9039–9051. https://doi.org/10039/C9NJ00332K
- [9] Wen, W.R., et al. Donor/acceptor complex of triphenylene and trinitrotoluene on Au (111): a scanning tunneling microscopy study. Chemical Communication, 47 (2011) 6915–6917. DOI: 10039/c1cc11358e
- [10] Salzillo, T., Campos, A., Mas-Torrent, M. Solution-processed thin films of a charge-transfer complex for ambipolar field-effect transistors. Journal of Materials Chemistry C, 7 (2019) 10257–10263. DOI https://doi.org/10039/C9TC03064F
- [11] Refat, M. S., et al. Spectroscopic characterizations on the N, N'-bis-alkyl derivatives of 1,4,6,8-naphthalenediimide charge-transfer complexes. Arabian Journal of Chemistry, 4 (2011) 83–97. DOI: 10016/j.arabjc.2010.06.024
- [12] AL-Attas, A. S., Habeeb, M. M., AL-Raimi, D. S. Synthesis and spectroscopic studies of charge-transfer complexes between chloranilic acid and some heterocyclic amines in ethanol.

 Journal of Molecular Structure, 928 (2009) 158–170.

 http://dx.doi.org/10016/j.molstruc.2009.03.025

- [13] Khawas, S., Laskar, S. Two New Spray Reagents for Detection of Amino Acids on Thin-Layer Plates. JPC-J Planar Chromatography, 16 (2003) 165–166. https://doi.org/10556/JPC6.2003.25S.
- [14] Margiotta, N., et al. Platinum-based antitumor drugs containing enantiomerically pure α -trifluoromethyl alanine as ligand. Journal of Medicinal Chemistry, 48 (2005) 7821–7828. https://doi.org/10021/jm0504003
- [15] Zhang. J., et al. Organic Donor–Acceptor Complexes as Novel Organic Semiconductors. Accounts of Chemical Research, 50 (2017) 1654–1662. DOI: 10021/acs.accounts.7b00124
- [16] AL-Attas, A. S., Habeeb, M. M., Basha, M. T. Spectrophotometric and Conductimetric Studies of Charge-transfer Complexes of Some Pyrimidine Derivatives with Chloranilic Acid as p-Acceptor in Methanol. World Journal of Chemistry, 2 (2007) 16-24.
- [17] Subhani, M. S., Bhatti, N. K., Mohammad, M., Khan, Tbitak, A. Y. Spectroscopic Studies of Charge-Transfer Complexes of 2,3-Dichloro-5,6-Dicyano-P-Benzo-Quinone. Turkish Journal of Chemistry, 24 (2000) 223 -230.
- [18] Asmaa, Ibrahim, A. Spectrophotometric studies of a charge-transfer complex of 8-hydroxyquinoline with 1,4-benzoquinone. African Journal of Pure and Applied Chemistry, 5 (2011) 507-514. DOI: 10.5897/AJPAC11.043
- [19] Ukoha, Pius, O. Spectrophotometric determination of 4-aminobenzoic acid using charge-transfer complexation, International Journal of ChemTech Research, 11 (2018) 370-376. http://doi.org/10.20902/IJCTR.201810244
- [20] Baharfar, M., Hillier, A. C., Mao, G. Charge-Transfer Complexes: Fundamentals and Advances in Catalysis, Sensing, and Optoelectronic Applications. Advanced Materials, 36 (2024) 2406083. https://doi.org/10.1002/adma.202406083

- [21] Baharfar, M., et al. Gas nanosensors for health and safety applications in mining. Nanoscale Advanced, 5 (2023) 5997-6016. DOI: 10.1039/D3NA00507K
- [22] Jeong, S., et al. Twisted Crystalline Organic Semiconductor Photodetectors. Advanced Functional Materials, 33 (2023) 2212531. https://doi.org/10.1002/adfm.202212531
- [23] An, L., et al. Organic Charge-Transfer Complexes for Near-Infrared-Triggered Photothermal Materials. Small Structures, 4 (2023) 2200220. DOI: 10.1002/sstr.202200220
- [24] Ali, M. M., et al. Synthesis, characterization, and toxicity evaluation of ciprofloxacinchloranilic acid charge transfer complexes: potential for anticancer applications. RSC Medicinal Chemistry, (2025) 29. doi: 10.1039/d5md00091b.
- [25] Krugly, E., et al. Decomposition of 2-naphthol in water using a non-thermal plasma reactor. Chemical Engineering Journal, 260 (2015) 188–198. https://doi.org/10016/j.cej.2014.08.098
- [26] Jie, L., Yu, C., Zhao, P., Chen, G. Comparative study of supported CuOx and MnOx catalysts for the catalytic wet air oxidation of naphthol. Applied Surface Science, 258 (2012) 9096–9102. https://doi.org/10016/j.apsusc.2012.06.022
- [27] Yang, S., Gao, M., Luo, Z. Adsorption of 2-naphthol on the organo-montmorillonites modified by Gemini surfactants with different spacers. Chemical Engineering Journal, 256 (2014) 39–50. https://doi.org/10016/j.cej.2014.07.004
- [28] Lin, Y. F., et al. Inhibitory effects of naphthols on the activity of mushroom tyrosinase. International Journal of Biological Macromolecules, 51 (2012) 32–36. https://doi.org/10016/j.ijbiomac.2012.04.026

- [29] Zhang, M., et al. Impacts of disinfection byproduct exposures on male reproductive health: Current evidence, possible mechanisms, and future needs. Chemosphere, 331 (2023) 138808. doi 10016/j.chemosphere.202338808.
- [30] Shin, H. S., Lim, H. H. Simultaneous determination of 2-naphthol and 1-hydroxy pyrene in urine by gas chromatography-mass spectrometry. Journal of Chromatography B, 879 (2011) 489–494. https://doi.org/10016/j.jchromb.2011.01.009
- [31] Kim, H., et al. Assay of 2-naphthol in human urine by high-performance liquid chromatography. Journal of Chromatography B, 734 (1999) 211–217. doi: 10016/s0378-4347(99)00350-3
- [32] Zhu, G., et al. Electrochemical sensor for naphthols based on gold nanoparticles/hollow nitrogen-doped carbon microsphere hybrids functionalized with SH—cyclodextrin. Analytica Chimica *Acta*, 723 (2012) 33–38. https://doi.org/10016/j.aca.2012.02.034
- [33] Zhong, S., et al. Determination of bisphenol A and naphthols in river water samples by capillary zone electrophoresis after cloud point extraction. Talanta, 85 (2011) 488–492. https://doi.org/10016/j.talanta.2011.04.009
- [34] Tsai, T. F., Lee, M. R. Liquid-phase microextraction combined with liquid chromatography-electrospray tandem mass spectrometry for detecting diuretics in urine. Talanta, 75 (2008) 658–665. https://doi.org/10016/j.talanta.20071.058
- [35] Farajzadeh, M. A., Feriduni, B., Mogaddam, M. R. A. Development of counter-current salting-out homogenous liquid-liquid extraction for isolation and preconcentration of some pesticides from aqueous samples. Analytica Chimica *Acta*, 885 (2015) 122–131. https://doi.org/10016/j.aca.2015.05.031

- [36] Cai, F., Zhu, W., Ibrahim, J. J., Xiao, G. Liquid extraction of polyhydric alcohols from water using [A336][SCN] as a solvent. *Journal of Chemical Thermodynamics*, 89 (2015) 35–40. https://doi.org/10016/j.jct.2015.04.033
- [37] Omidi, F., Behbahani, M., Bojdi, M. K., Shahtaheri, S. J. Solid phase extraction and trace monitoring of cadmium ions in environmental water and food samples based on modified magnetic nanoporous silica. Journal of Magnetism and *Magnetic* Materials, 395 (2015) 213–220. https://doi.org/10016/j.jmmm.2015.07.093
- [38] MJ Frisch, et al. Gaussian 09, Revision D.01, Gaussian, Inc., Wallingford CT (2009).
- [39] Dennington, R., Keith, T., Millam, J. in ed. S Mission, Version 5, Semichem Inc., KS (2009).
- [40] Becke, A. D. Density-functional thermochemistry. III. The role of exact exchange. Journal of *Chemical Physics*, 98 (1993) 5648-5652. https://doi.org/10063/1.464913.
- [41] Hehre, W. J., Ditchfield, R., Stewart, R. F. Self-Consistent Molecular-Orbital Methods.

 12. Further Extensions of Gaussian-Type Basis Sets for Use in Molecular Orbital Studies of Organic Molecules. Journal of *Chemical Physics*, 56 (1972) 2257-2261.

 https://doi.org/10063/1677527
- [42] Runge, E., Gross, E. K. U. Density-Functional Theory for Time-Dependent Systems. *Physical Review Letters*, 52 (1984) 997-1000. https://doi.org/10103/PhysRevLett.52.997
- [43] Ganesh, K., Balraj C., Satheshkumar, A., Elango, K. P. Spectroscopic studies on the formation of charge-transfer complexes of l-phenylalanine with 2,3,5-trichloro-6-alkoxy-1,4-benzoquinones in aqueous medium. Arabian Journal of Chemistry, 12 (2019) 503-514. https://doi.org/10016/j.arabjc.20140.020.

- [44] Teimouri, A. N., Chermahini, A., Taban K., Dabbagh, H. Experimental and CIS, TD-DFT, ab Initio Calculations of Visible Spectra and the Vibrational Frequencies of Sulfonylazide-Azoic Dye. Spectrochimica Acta Part A, 72 (2009) 369-377. http://dx.doi.org/10016/j.saA20080.006
- [45] Rahman, H., et al. Spectroscopic and DFT studies of the charge-transfer complexation of iodine with aniline and its derivatives in carbon tetrachloride medium. Journal of Molecular Liquids, 351 (2022) 118667. https://doi.org/10016/j.molliq.202218667.
- [46] Veit, M., et al. Predicting molecular dipole moments by combining atomic partial charges and atomic dipoles. Journal of *Chemical Physics*, 153 (2020) 024113. **DOI**: 10063/5.0009106.
- [47] Heitzer, H. M., Marks, T. J., Ratner, M. A. Molecular Donor-Bridge-Acceptor Strategies for High-Capacitance Organic Dielectric Materials. Journal of the American Chemical Society, 137 (2015) 7189-7196. DOI: 10021/jacs.5b03301
- [48] Sutradhar, T., Misra, A. The role of π -linkers and electron acceptors in tuning the nonlinear optical properties of BODIPY-based zwitterionic molecules. RSC Advances;10 (2020) 40300-40309. DOI: 10039/d0ra02193h.
- [49] Fleming, I. Frontier Orbitals and Organic Chemical Reactions, John Wiley and Sons, New York, (1976).
- [50] Beigloo, N. A. B., Rezvan, V. H., Ebrahimzadeh-Rajaei Gh, Shamel, A. Spectral Measurements of a Novel Charge Transfer Complex Formed by a Heterocyclic Aromatic Amine and 1,4-Dinitrobenzene: A Combined Experimental and DFT Approach. Physical Chemistry Research, 13(4) (2025) 701-720, DOI: 10.22036/pcr.2025.529463.2695

- [51] Rezvan, V. H., Barani Pour S., Sardroodi, J. J. Molecular structures and optical properties of Schiff bases derived from pyrrole alkyl ketones and 1-aminophethalazine: DFT calculations. Results in Chemistry, 12 (2024) 101907. https://doi.org/10.1016/j.rechem.2024.101907.
- [52] Rezvan, V. H., Charge transfer complexes: a review survey. Results in Chemistry, 17 (2025) 102600 https://doi.org/10016/j.rechem.202502600
- [53] Prasad, O., et al. Molecular structure and vibrational study on 2,3-dihydro-1H-indene and its derivative 1H-indene-1,3(2H)-dione by density functional theory calculations. Journal of Molecular Structure THEOCHEM, 940 (2010) 82–86. https://doi.org/10016/j.theochem.20090.011
- [54] Ghrieb, H., Kadri, M. Spectroscopic and computational investigation of a novel charge-transfer complex via hydrogen bonding between β-cyclodextrin with DDQ and TCNE: NBO, AIM, NLO, and DFT analysis. Egyptian Journal of Chemistry, 65(8) (2022) 247-262. doi 10.21608/ejchem.202108057.4943
- [55] Varukolu, M., et al. New Charge-transfer Complex between 4-Dimethylaminopyridine and DDQ: Synthesis, Spectroscopic Characterization, DNA Binding Analysis, and Density Functional Theory (DFT)/Time-Dependent DFT/Natural Transition Orbital Studies. *ACS Omega*, 7 (1) (2022) 810-822. DOI: 10021/acsomegac05464
- [56] Kaya, T., Selçuki, C., Acar, N. A DFT and TDDFT investigation of interactions between 1-hydroxypyrene and aromatic amino acids. Computational Theoretical Chemistry, 1073 (2015) 9-19. https://doi.org/10016/j.comptc.2015.09.009
- [57] Weinhold, F., Landis, C. R. Natural Bond Orbitals. Journal of the American Chemical Society, 127 (2005) 14057-14067. DOI: 10021/ja0531974

- [58] Glendening, E. D., Landis, C. R., Weinhold, F. (NBO 7.0): Natural Bond Orbital Analysis Program. Journal of Computational Chemistry, 40(3) (2019) 223-231. DOI: 10002/jcc.25456.
- [59] Weinhold, F., Landis, C. R. Valency and Bonding: A Natural Bond Orbital Donor-Acceptor Perspective. Cambridge University Press. (2001).
- [60] Lin, H., et al. Reversible Switching of Charge-transfer at the Graphene-Mica Interface with Intercalating Molecules. ACS Nano, 14(9) (2020) 11594-11604. DOI: 10021/acsnano.0c04144.
- [61] Tsuzuki, S., Uchimaru, T., Ono, T. Origin of attraction in p-benzoquinone complexes with benzene and p-hydroquinone. Physical Chemistry Chemical Physics, 19(34) (2017) 23260-23267. DOI: 10039/c7cp03712k.
- [62] Raafat, B. M., Refat, M. S., Gaber, A. Increasing the Efficacy of Seproxetine as an Antidepressant Using Charge-Transfer Complexes. Molecules, 27(10) (2022) 3290. doi: 10.3390/molecules27103290.
- [63] Rezvan, V. H., Barani Pour, S., Behrooz, N. J., Sardroodi, J. J. A computational perspective on the changes made in the structural, optical, and electronic properties of melamine and picric acid/quinol with the formation of charge transfer complexes. Structural Chemistry, (2025) https://doi.org/10007/s11224-025-02506-6